Ritz-type variable speed of light (VSL) cosmology

Santosh Devasia[a)]
Department of Mechanical Engineering, University of Washington, Stevens Way, Box 352600, Seattle, Washington 98195-2600, USA

(Received 22 February 2014; accepted 3 September 2014; published online 23 September 2014)

Abstract: This article develops a variable-speed-of-light (VSL) cosmology model. VSL has been used previously in cosmology models, in which either (i) the physical constants vary over time or (ii) the Lorentz invariance is broken locally. VSL is also allowed in the relative-velocity-based approach, which is used in the current article to propose a VSL-type cosmology model. Additionally, the article evaluates the model's potential to match current cosmological observations. © *2014 Physics Essays Publication.* [http://dx.doi.org/10.4006/0836-1398-27.4.523]

Résumé: Cet article développe un modèle cosmologique basé sur une vitesse de la lumière variable (VSL). La VSL a été utilisée auparavant par des modèles cosmologiques, dans lesquels (i) les constantes physiques varient au cours du temps, ou (ii) l'invariance de Lorentz est localement violée. La VSL est également autorisée dans l'approche basée sur une vitesse relative, qui est utilisée dans le présent article pour proposer un modèle cosmologique de type VSL. En outre, cet article examine le potentiel du modèle pour égaler les observations cosmologiques actuelles.

Key words: Cosmology; Ritz; Time Dilation; Farther Dimmer; Superluminal Ejecta; VSL.

I. INTRODUCTION

The large number of anomalies in cosmological observations has led to substantial interest in alternatives to the standard big-bang type cosmology, e.g., Refs. 1–5. The main contribution of this article is to propose a Ritz-type, variable-speed-of-light (VSL) cosmology model where the velocity of light is dependent on source velocity. A recent review of Ritz's approach shows that the astronomical observations that were initially thought to be contradictory were later found to be consistent.[6] It is noted that VSL has been used, previously, in cosmology models,[7] where physical constants (such as the gravitational constant) are allowed to vary over time. The relationships between the temporal variations of the different physical constants can be determined to match physical observations such as relativistic electromagnetism. The current article evaluates the potential for an alternate (Ritz-type VSL) model to match cosmological observations and explain current anomalies.

In Ritz-type models, VSL is assumed wherein the velocity of the source augments the speed of light. Several researchers had suggested investigating astronomical data to test Ritz-type models—such astronomical observations (e.g., irregularities in observations of double-star system) that were initially thought to be contradictory were later found to be consistent.[6] Nevertheless, there remained several challenges such as the inability to (i) explain Fresnel drag and (ii) the lack of an accompanying electromagnetic theory, which would require modification of Maxwell's equations. These issues were recently addressed in Ref. 8, which extends Maxwell's equations to enable a Ritz-type VSL. There are two main changes—(i) the partial time derivative in Maxwell's equations is replaced by the total time derivative and (ii) the electromagnetic force depends on the relative velocity between particles, which is a modification of Weber's approach.[9] The resulting relative-velocity-based model[8] not only captures relativity effects in optics (such as the Fresnel drag and transverse Doppler effects) but also explains apparent discrepancies between predicted and measured energy in: (i) the absorption of high-energy particles in cloud chambers[10] and (ii) the average energy determination of the X-ray spectrum using magnetic fields.[11] Based on these efforts, the current article proposes a Ritz-type VSL cosmology model.

The article begins by showing (in Sec. II) that the proposed model can be used to derive the standard Hubble law, and is consistent with the time dilation seen in current cosmological observations.[12] Then, periodic photosphere motions are investigated for its effect on VSL cosmology and its ability to match stellar observations in Sec. III. Issues in quasar observations such as the apparent lack of time dilation in quasar light curves,[13] even though time dilation has been observed in supernovae (SNe) light curves,[12] are studied in Sec. IV. The model is used to also investigate, in Sec. IV, observations that (i) link some quasars with low redshift galaxies[14,15] and (ii) indicate the presence of superluminal ejecta.[16] Consistency of the model with recent farther–dimmer relation[17] in SNe observations is shown in Sec. V. The proposed model leads to temporal-and-spatial distortions in cosmological observations—the impact of such distortions is discussed in Sec. VI. Finally, potential large-scale anisotropies, e.g., in the Hubble constant, are discussed in Sec. VII, which is followed by the conclusions section.

a)devasia@u.washington.edu

II. DERIVATION OF THE HUBBLE LAW

A. The model

The current article considers a big-bang-type model where the universe (containing astrophysical objects) is a uniformly expanding spherical shell (geometry axiom), which is similar to Newtonian cosmology models, e.g., Ref. 18. However, in contrast to the Newtonian cosmology model where the expansion speed increases linearly with the distance from the center,[18] the expansion speed is constant in the current model. Nevertheless, it is shown that even with a constant expansion speed, the Ritz-type VSL model is consistent the farther–dimmer relation seen in recent SNe-based observations.[17]

Consider light emitted in all directions at the standard speed of light c and frequency υ_e by an emitter e when it is at the location e_e at time t_1 as shown in Fig. 1. According to the geometry axiom, the emitter is moving at constant speed V, i.e., velocity $V\underline{r}_e$ with respect to an inertial frame I_a at a central position a as shown in Fig. 1, where $\underline{r}_e$ is a fixed, unit vector.

After time $\Delta t_{1,2}$, let the light reach an observer o at location o_o at time $t_2 = t_1 + \Delta t_{1,2}$, where the observer is moving at constant velocity $V\underline{r}_o$ with respect to the inertial frame I_a and $\underline{r}_o$ is a fixed, unit vector. With respect to the emitter inertial frame I_e (moving with the emitter as shown in Fig. 1), during the time interval $\Delta t_{1,2}$, light has traveled a distance $d_o = d(e_o, o_o) = c\Delta t_{1,2}$, i.e., reached a shell of radius d_o centered at e_o at time t_2.

The speed c_o of the light observed in an inertial frame I_o on the observer o (at location o_o) is given by

$$c_o\underline{y} = V_e\underline{r}_e + c\underline{y} - V_o\underline{r}_o = V\underline{r}_e + c\underline{y} - V\underline{r}_o, \tag{1}$$

where $\underline{y}$ is a fixed unit vector. As in Ritz-type models, the velocity of light $\underline{c}$ is added to the velocity of the source $\underline{v}_s$, i.e., $\underline{c} + \underline{v}_s$ to find the propagation velocity (the velocity axiom) in the relative-velocity-based approach. Although the proposed approach is different from the tired-light-type hypothesis, e.g., Ref. [1], the current model also results in a distance–redshift relation that matches the Hubble law as shown below.

The magnitude c_o of the observed light velocity can be found using the similar triangles $\Delta(ae_eo_e)$ and $\Delta(ae_oo_o)$, to obtain the following relationship between: (i) the distance $R = d(a, e_o) = d(a, o_o)$ from the center a to the observer and emitter at observation time t_2 and (ii) $d_e = d(e_e, o_e)$ the distance between observer and emitter at the emission time instant t_1

$$\frac{d_e}{d_o} = \frac{c_o\Delta t_{1,2}}{c\Delta t_{1,2}} = \frac{c_o}{c} = \frac{R - V\Delta t_{1,2}}{R} = \frac{R - V\left(\frac{d_o}{c}\right)}{R} = 1 - \frac{V}{Rc}d_o, \tag{2}$$

where $d_e = c_o\Delta t_{1,2}$ since this initial distance at time t_1 is covered at speed c_o in the observer frame I_o. Note that the observed light speed c_o is less than the standard speed of light c from Eq. (2) since $d_e \le d_o$, i.e.,

$$c_o \le c. \tag{3}$$

B. Time dilation, red shift, and energy reduction

The cosmological expansion and the reduction in observed light speed result in three effects discussed below: (i) perceived time dilation; (ii) redshift; and (iii) energy reduction.

1. Perceived time dilation

The emitter is seen to move away from the observer (in the observer frame of reference I_o) at a speed $V_{e,o}$ described by, from Eq. (1),

$$V_{e,o}\underline{y} = V\underline{r}_e - V\underline{r}_o = (c - c_o)\underline{y}. \tag{4}$$

Consider two photons emitted at time instants t_1 and $t_1 + t_e$, which move toward the observer at speed c_o in the observer frame of reference I_o. During the time interval t_e, the distance $d_e = d(e_e, o_e)$ between the emitter and the observer

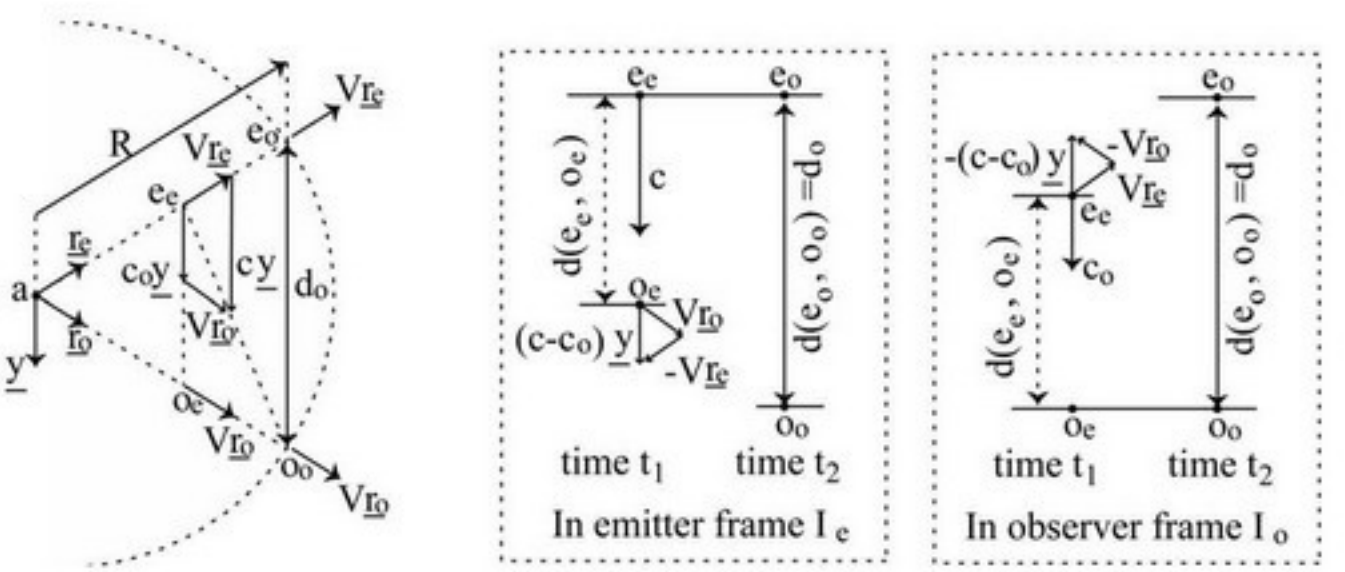

FIG. 1. VSL based on reference frame: (left) reference frame at center of cosmological shell; (middle) reference frame associated with the emitter; and (right) reference frame associated with the observer. Light emitted from point e_e at time t_1 reaches observer at o at time t_2, after time $\Delta t_{1,2} = t_2 - t_1$. Distances at observation time t_2 of the emitter and observer from the center a are $d(a, e_o) = R$ and $d(a, o_o) = R$, respectively. Both emitter and observer are moving away from the center a at constant speed $V_e = V_o = V$. Distance between observer and emitter at emission time t_1 is $d(e_e, o_e) = d_e$ and at observation time t_2 is $d(e_o, o_o) = d_o$.

has increased by $V_{e,o}t_e$. Hence the time interval t_o between the observations of the two photons (in the observer frame I_o) is given by, from Eq. (4),

$$t_o = \left(t_e + \frac{d_e + V_{e,o}t_e}{c_o}\right) - \frac{d_e}{c_o} = \left[t_e + \frac{(c - c_o)t_e}{c_o}\right] = \frac{c}{c_o}t_e. \quad (5)$$

Therefore, a time interval t_e in the emitter frame appears (optically) as a dilated time interval t_o in the observer frame with

$$t_o = \frac{c}{c_o}t_e \geq t_e, \quad (6)$$

since $c \geq c_o$ by Eq. (3). Consequently, events in the emitter frame I_e appear (optically) to occur at a slower rate in the observer frame I_o leading to a perceived time dilation.

2. Redshift

The observed frequency υ_o is reduced with respect to the emitted frequency υ_e due to the Doppler effect. For example, $N_\upsilon = \upsilon_e t_e$ pulses sent at frequency υ_e in time t_e from the emitter are received at the observer in time t_o, as in Eq. (6). Therefore, the observed frequency υ_o is, by using Eq. (6)

$$\upsilon_o = \frac{N_\upsilon}{t_o} = \frac{t_e}{t_o}\upsilon_e = \frac{c_o}{c}\upsilon_e, \quad (7)$$

which corresponds to a redshift $z \geq 0$ given by

$$z = \frac{\upsilon_e - \upsilon_o}{\upsilon_o} = \frac{\upsilon_e}{\upsilon_o} - 1 = \frac{c}{c_0} - 1, \quad (8)$$

that can be rewritten as

$$1 + z = \frac{c}{c_0}. \quad (9)$$

Moreover, the distance d_o in Eq. (2) can be rewritten in terms of the redshift z as

$$d_o = \frac{Rc}{V}\left(1 - \frac{c_o}{c}\right) = \frac{Rc}{V}\left(1 - \frac{1}{1+z}\right) = \frac{Rc}{V}\left(\frac{z}{1+z}\right), \quad (10)$$

and the observed frequency in Eq. (7) can be rewritten as

$$\upsilon_o = \frac{c_o}{c}\upsilon_e = \frac{1}{1+z}\upsilon_e. \quad (11)$$

Note that the time dilation expression can be written in terms of the red shift from Eqs. (6) and (9) as

$$t_o = \left(\frac{c}{c_o}\right)t_e = (1+z)t_e. \quad (12)$$

The time dilation of $1 + z$ is consistent with cosmological observations such as the time broadening of SNe light curves.[12]

3. Energy reduction

The energy of a photon is reduced in the observer inertial frame I_o when compared to the emitter inertial frame I_e due to the reduction in the photon frequency between the two frames, from υ_e to υ_o given by Eq. (11). The ratio of perceived energy E_o (of photons) in the observer frame to the energy E_e (of the corresponding photons) in the emitter frame is given by

$$\frac{E_o}{E_e} = \frac{h\upsilon_o}{h\upsilon_e} = \frac{1}{1+z}, \quad (13)$$

where h is the Planck constant. Note that in addition to the change in the observed energy of the light-quanta due to a reduction of the observed frequency, as in Eq. (13), the observed energy is reduced by the perceived time dilation, as in Eq. (12), since it leads to a change in the arrival rate of light-quanta. Hubble suggested both these effects as corrections in Ref. 19.

C. Luminosity distance and red shift

Let L_e be the total energy of photons emitted from e_e per unit time. Then, the energy $L_e\Delta t_e$ emitted in a small time interval Δt_e is spread over a shell of radius d_o centered at point e_o after time $\Delta t_{1,2}$ as in the middle plot of Fig. 1. The resulting energy per unit surface area E_e of this shell (in the emitter inertial frame I_e) is given by, from Eq. (10),

$$E_e = \frac{L_e}{4\pi d_o^2}\Delta t_e = \frac{L_e}{4\pi\left(\frac{Rc}{V}\right)^2\left(\frac{z}{1+z}\right)^2}\Delta t_e. \quad (14)$$

In this same situation, the energy per unit surface area E_o observed at o_2 in the dilated-time interval Δt_o (in the observer inertial frame I_o) is, from Eqs. (12)–(14),

$$E_o = \frac{E_e}{1+z} = \frac{L_e}{4\pi\left(\frac{Rc}{V}\right)^2\left(\frac{z^2}{1+z}\right)}\Delta t_e = \frac{L_e}{4\pi\left(\frac{Rc}{V}\right)^2\left(\frac{z^2}{1+z}\right)}\frac{\Delta t_o}{1+z} = \frac{L_e\Delta t_o}{4\pi\left(\frac{Rc}{V}z\right)^2}. \quad (15)$$

Then, the observed brightness B_o (i.e., energy per unit area per unit time in the observer inertial frame I_o at O_o) is given by

$$B_o = \frac{E_o}{\Delta t_o} = \frac{L_e}{4\pi\left(\frac{Rc}{V}z\right)^2} = \frac{L_e}{4\pi(d_L)^2}, \quad (16)$$

where the observed luminosity distance d_L increases linearly with the redshift z as

$$d_L = \frac{R}{V}cz = (H^{-1})cz, \quad (17)$$

which can be rewritten as (the Hubble law)

$$V_{\text{apparent}} = cz = Hd_{\text{L}}, \tag{18}$$

with V_{apparent} being the apparent speed away from the observer (based on the redshift z) and

$$H = \frac{V}{R}, \tag{19}$$

is the Hubble constant.

D. Relation between the different distances

The model yields the expected relation between angular distance, proper distance and the observed luminosity distance d_{L}, as described below. In the observer inertial frame I_{o}, the emission is initiated at distance d_{e}—although the emitter is then seen to move away at speed $(c - c_{\text{o}})$. Therefore, the angle θ_{e} of the emitter in the sky and the perceived size S_{e} are related to the angular distance d_{e} as $S_{\text{e}} = \theta_{\text{e}} d_{\text{e}}$. The distance d_{o} between the emitter and observer at the observation time is considered as the proper distance at the time of observation. The luminosity distance d_{L} and the proper distance d_{o} are related from Eqs. (10) and (17),

$$d_{\text{o}} = \frac{Rc}{V} z \left(\frac{1}{1+z}\right) = \frac{d_{\text{L}}}{1+z}. \tag{20}$$

The angular distance d_{e} and the proper distance d_{o} are related from Eqs. (2) and (9),

$$d_{\text{e}} = \frac{c_{\text{o}}}{c} d_{\text{o}} = \frac{d_{\text{o}}}{1+z}, \tag{21}$$

resulting in the following relation between the luminosity distance d_{L}, the proper distance d_{o}, and the angular distance d_{e}:

$$d_{\text{L}} = (1+z) d_{\text{o}} = (1+z)^2 d_{\text{e}}. \tag{22}$$

III. EFFECT OF VSL ON STELLAR OBSERVATIONS

The time dilation is affected by the speed and radius of the photosphere; the associated distortion of the light curves from nearby stars is studied in this section.

A. Periodic photosphere motion

Consider a nearby star at distance $d_{\text{e,o}}$, for which cosmological expansion effects (such as time dilation) are negligible. This allows the following analysis to focus on just the effect of the velocity addition on the speed of light. Let the motion of the photosphere be periodic and continuous, and consider one time period, i.e., time interval $[t_{\text{e},i}, t_{\text{e},i} + T_{\text{p}}]$, where T_{p} is time period of the photosphere motion. For any time instant $t = t_{\text{e},i} + t_{\text{e}} \in [t_{\text{e},i}, t_{\text{e},i} + T_{\text{p}}]$, i.e., for the shifted emission time $t_{\text{e}} = (t - t_{\text{e},i}) \in [0, T_{\text{p}}]$, let the acceleration $a_{\text{p}}(t_{\text{e}}) = c\dot{\beta}_{\text{p}}(t_{\text{e}})$ of the photosphere be given by $\dot{\beta}_{\text{p}}(t_{\text{e}}) = f_{\text{p}}(t_{\text{e}}) + C_a$ where $f_{\text{p}}(t_{\text{e}})$ is a periodic function with time period T_{p} in the emitter frame I_{e}. Note that the functions are described in terms of the shifted, emission time t_{e}. The constant C_a is chosen such that the speed $v_{\text{p}} = c\beta_{\text{p}}$ of the photosphere is periodic, and continuous at the endpoints of the time interval $t_{\text{e}} \in [0, T_{\text{p}}]$, e.g.,

$$\begin{aligned}\frac{v_{\text{p}}(T_{\text{p}})}{c} - \frac{v_{\text{p}}(0)}{c} &= \beta_{\text{p}}(T_{\text{p}}) - \beta_{\text{p}}(0) = \int_0^{T_{\text{p}}} \dot{\beta}_{\text{p}}(t_{\text{e}}) dt_{\text{e}} \\ &= T_{\text{p}} C_a + \int_0^{T_{\text{p}}} f_{\text{p}}(t_{\text{e}}) dt_{\text{e}} = 0.\end{aligned} \tag{23}$$

Moreover, the initial velocity $v_{\text{p}}(0)$ is chosen to ensure that the radial photosphere position $r_{\text{p}}(t_{\text{e}})$ is periodic, and continuous at the endpoints of the time interval $t_{\text{e}} \in [0, T_{\text{p}}]$, e.g.,

$$\frac{r_{\text{p}}(T_{\text{p}})}{c} - \frac{r_{\text{p}}(0)}{c} = \int_0^{T_{\text{p}}} \beta_{\text{p}}(t_{\text{e}}) dt_{\text{e}} = 0. \tag{24}$$

An example photosphere trajectory is shown in Fig. 2.

B. Observation and emission time intervals

Consider two photons emitted at time instants $t = t_{\text{e},i}$ and $t = t_{\text{e},i} + t_{\text{e}}$, which move toward the observer at speeds $c + c\beta_{\text{p}}(0)$ and $c + c\beta_{\text{p}}(t_{\text{e}})$, respectively, in the emitter frame I_{e}. Let the photons reach an observer o (at a distance $d_{\text{e,o}}$) at the two time instants $t = t_{\text{o},i}$ and $t = t_{\text{o},i} + t_{\text{o}}$, respectively, where

$$t_{\text{o},i} = t_{\text{e},i} + \frac{d_{\text{e,o}} - r_{\text{p}}(0)}{c + c\beta_{\text{p}}(0)}, \tag{25}$$

$$t_{\text{o},i} + t_{\text{o}} = t_{\text{e},i} + t_{\text{e}} + \frac{d_{\text{e,o}} - r_{\text{p}}(t_{\text{e}})}{c + c\beta_{\text{p}}(t_{\text{e}})}, \tag{26}$$

and the shifted observer time $t_{\text{o}} = (t - t_{\text{o},i})$ can be found by subtracting the above two expressions as

$$\begin{aligned}t_{\text{o}} &= t_{\text{e}} + \frac{d_{\text{e,o}}}{c}\left[\frac{1}{1+\beta_{\text{p}}(t_{\text{e}})} - \frac{1}{1+\beta_{\text{p}}(0)}\right] \\ &\quad - \frac{1}{c}\left[\frac{r_{\text{p}}(t_{\text{e}})}{1+\beta_{\text{p}}(t_{\text{e}})} - \frac{r_{\text{p}}(0)}{1+\beta_{\text{p}}(0)}\right] \\ &= t_{\text{e}} - \frac{d_{\text{e,o}}}{c}\frac{\beta_{\text{p}}(t_{\text{e}}) - \beta_{\text{p}}(0)}{[1+\beta_{\text{p}}(t_{\text{e}})][1+\beta_{\text{p}}(0)]} \\ &\quad - \frac{1}{c}\left[\frac{r_{\text{p}}(t_{\text{e}})}{1+\beta_{\text{p}}(t_{\text{e}})} - \frac{r_{\text{p}}(0)}{1+\beta_{\text{p}}(0)}\right].\end{aligned} \tag{27}$$

For periodic emissions (with period T_{p}, which is assumed to be large compared to the time for light to travel across the photosphere radius, i.e., r_{p}/c) and for small photosphere speeds (i.e., small β_{p}), Eq. (27) can be simplified to

$$\begin{aligned}t_{\text{o}} &\approx t_{\text{e}} - T_{\text{p}}\left(\frac{\beta_{\text{p,max}} d_{\text{e,o}}}{cT_{\text{p}}}\right)\left[\frac{\beta_{\text{p}}(t_{\text{e}}) - \beta_{\text{p}}(0)}{\beta_{\text{p,max}}}\right], \\ &= t_{\text{e}} - T_{\text{p}}\Gamma_{\text{p}}\left[\frac{\beta_{\text{p}}(t_{\text{e}}) - \beta_{\text{p}}(0)}{\beta_{\text{p,max}}}\right],\end{aligned} \tag{28}$$

where $c\beta_{\text{p,max}}$ corresponds to the maximum absolute value of the photosphere speed. Without photosphere motion, the

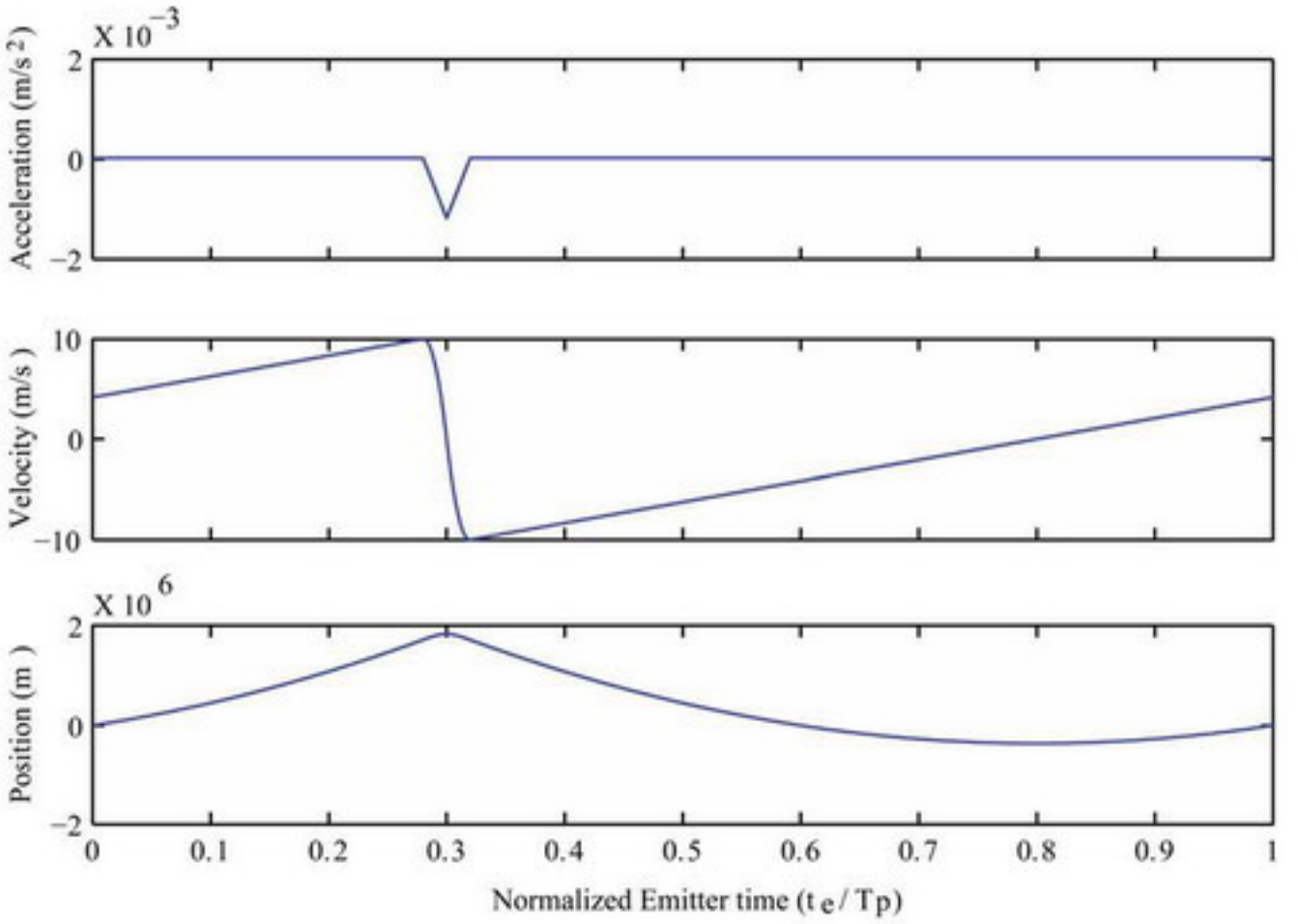

FIG. 2. (Color online) Example periodic photosphere motion for emitter time $t_e \in [0, T_p]$. The acceleration varies linearly in the normalized time intervals $t_e/T_p \in [0.28, 0.3)$ and $t_e/T_p \in [0.3, 0.32)$, and is constant elsewhere. Specific values of the acceleration are $a_p = 2.4 \times 10^{5}\text{m/s}^2$ at $t_e/T_p = 0$ and $a_p = -1.2 \times 10^{3}\text{m/s}^2$ at $t_e/T_p = 0.3$.

observation and emission time intervals would be equal, i.e., $t_o = t_e$. However, for the same emission time interval t_e, the observation time interval t_o is smaller if the photosphere speed, β_p is larger since it takes less time for the emission to travel the distance $d_{e,o}$.

For example, the observation and emission time intervals t_o and t_e, as in Eq. (28), are compared in Fig. 3 for the photosphere motion in Fig. 2. The parameter Γ_p in Eq. (28) is chosen to be $\Gamma_p = 4 \times 10^{-4}$, which corresponds to a time period T_p of 10 days, distance d of 100 parsecs, and maximum (absolute) photosphere speed of $v_p = 10$ m/s. Note that other combinations of these terms can also lead to the same parameter Γ_p value. The observation and emission time intervals t_o and t_e are similar. Therefore, for clarity, one of the curves (t_o/T_p) is displaced upward in the top plot of Fig. 3. Moreover, the difference $(t_o - t_e)/T_p$ is shown in the bottom plot in Fig. 3.

C. Brightness variation follows photosphere acceleration

If the energy-emission rate from the star were constant, then without photosphere motion, the observed brightness B_o would be uniform, i.e., $B_o(t_o) = B^*$. However, with photosphere motion, photons that are emitted in evenly spaced intervals of time will not be observed in evenly spaced intervals of time due to changes in the time t_o between observations as quantified in Eq. (28). The variation in the observed brightness is numerically evaluated by discretizing the emission times into small intervals, and mapping the emitted photons into discretized observation time intervals. The resulting observed brightness B_o, with and without photosphere motion, is compared in Fig. 4.

With a small photosphere motion, the variation of the observed brightness B_o (in Fig. 4) has a similar trend as the photosphere acceleration a_p (in Fig. 2). To clarify this, photons observed during a small time interval Δt_o around the shifted, observation time t_o could be related to those from the associated emission time interval Δt_e, from Eq. (28),

$$\begin{aligned}\Delta t_o &= \left[\frac{dt_o}{dt_e}(t_e)\right]\Delta t_e = \left[1 - \left(\frac{\Gamma_p T_p}{\beta_{p,\max}}\right)\frac{d\beta_p}{dt_e}(t_e)\right]\Delta t_e, \\ &= \left[1 - \left(\frac{\Gamma_p T_p}{c\beta_{p,\max}}\right)a_p(t_e)\right]\Delta t_e \\ &= \left[1 - \left(\frac{d_{e,o}}{c^2}\right)a_p(t_e)\right]\Delta t_e.\end{aligned} \tag{29}$$

Hence, the observed brightness, with photosphere motion, is related to the observed brightness B^* without photosphere motion through

$$B_o(t_o) = B^*\frac{\Delta t_e}{\Delta t_o} = B^*\frac{1}{1 - \left(\frac{d_{e,o}}{c^2}\right)a_p(t_e)}, \tag{30}$$

where the shifted observation and emission times t_o and t_e are related by Eq. (28). In the logarithmic scale, for sufficiently small photosphere motions, i.e., sufficiently small acceleration a_p,

$$\begin{aligned}\log_{10}[B_o(t_o)] &= \log_{10}[B^*] - \log_{10}\left[1 - \left(\frac{d_{e,o}}{c^2}\right)a_p(t_e)\right], \\ &\approx \log_{10}[B^*] + \left[\frac{1}{\ln(10)}\left(\frac{d_{e,o}}{c^2}\right)\right]a_p(t_e),\end{aligned} \tag{31}$$

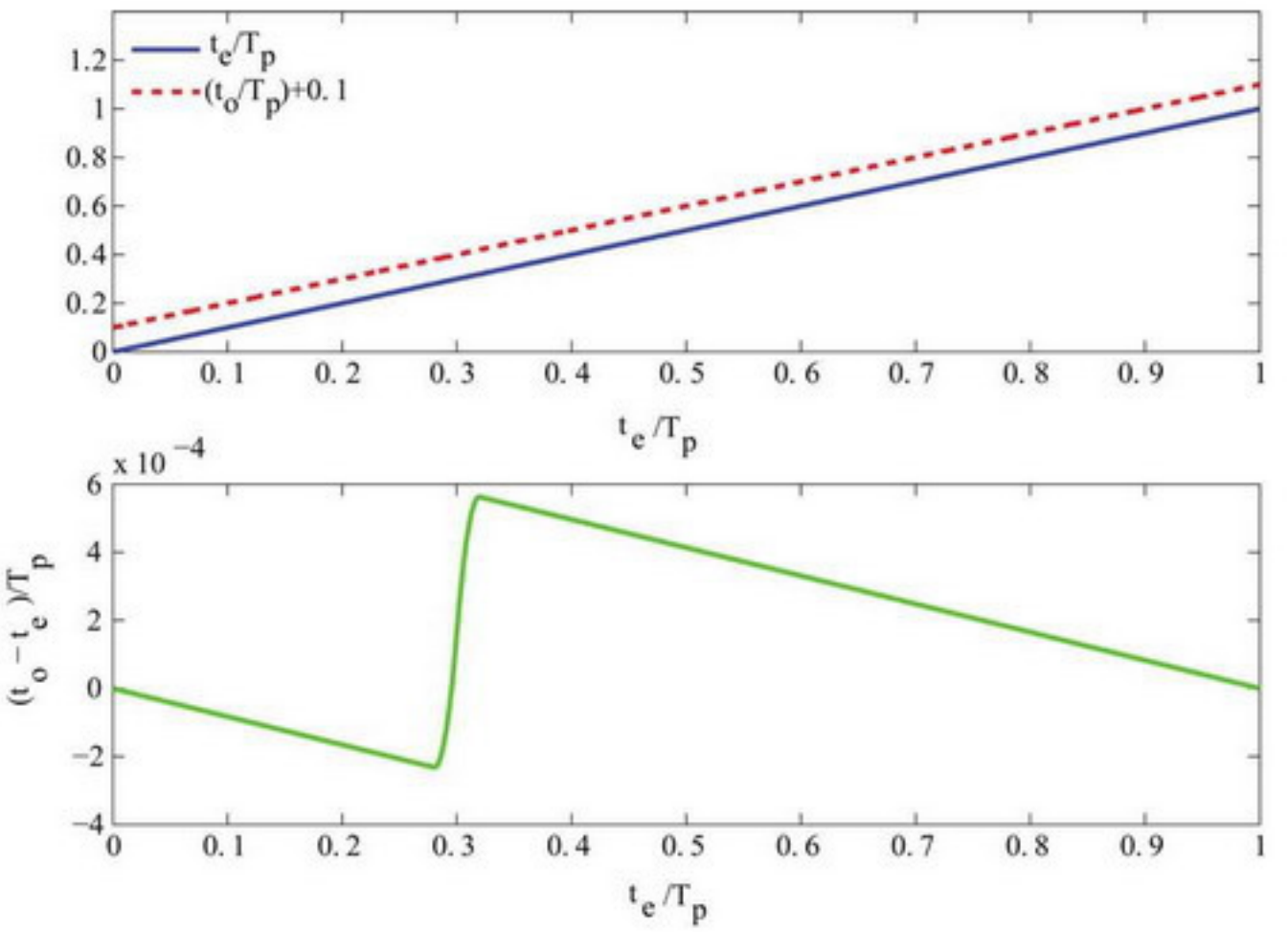

FIG. 3. (Color online) Comparison of normalized, observation time interval (t_o/T_p) in Eq. (28) with parameter $\Gamma_p = 4 \times 10^{-4}$, and normalized, emission time interval (t_e/T_p) for the photosphere motion in Fig. 2.

which results in

$$\log_{10}\left[\frac{B_o(t_o)}{B^*}\right] = \left[\frac{1}{\ln(10)}\left(\frac{d_{e,o}}{c^2}\right)\right] a_p(t_e) \propto a_p(t_e). \quad (32)$$

Thus, the variation in the observed brightness $\log_{10}[B_o(t_o)]$ (i.e., the light curve) reflects the photosphere acceleration when the photosphere motion is small and slowly varying. This similarity in the observed light curves is seen in Fig. 4, which compares the numerically computed brightness (e.g., photosphere motion) and the limit case in Eq. (32) for small, sufficiently slowly varying, photosphere motions.

Other types of photosphere acceleration (e.g., sinusoidal) are possible. The possible set of acceleration time patterns depends on the type of photosphere vibrations and the stellar dynamics. The difference between the shifted observation and emission times, t_o and t_e, increases with the parameter Γ_p in Eq. (28). Hence, the brightness variation can change substantially from the limit case, in Eq. (32). To illustrate, the parameter Γ_p is increased from $\Gamma_p = 4 \times 10^{-4}$ to $\Gamma_p = 4$ and the resulting brightness variation (light curves) over a time period is shown in Fig. 5, which has similar patterns to typical light curves of binary stars.

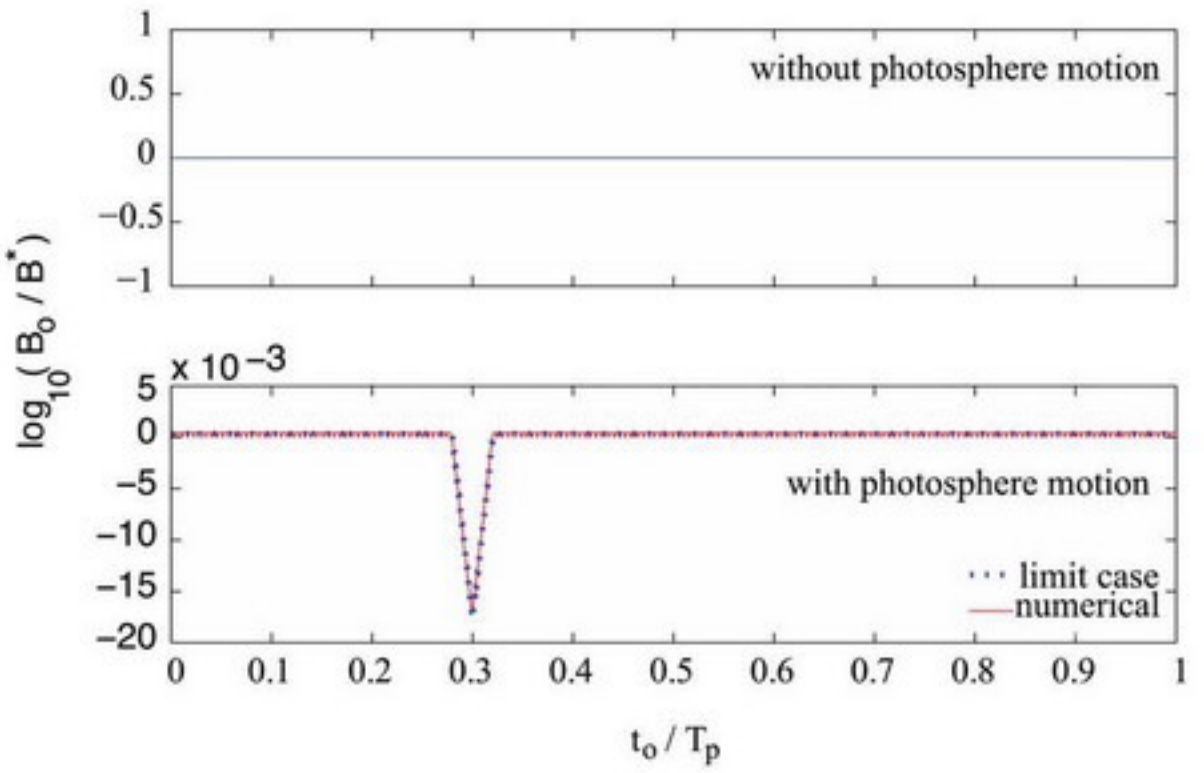

FIG. 4. (Color online) Comparison of observed brightness, without (top) and with (bottom) photosphere motion. The observed brightness B_o has a similar trend as the photosphere acceleration a_p (in Fig. 2) even though the energy-emission rate is uniform. Moreover, the observed brightness is close to the limit case for the example photosphere motion in Fig. 2.

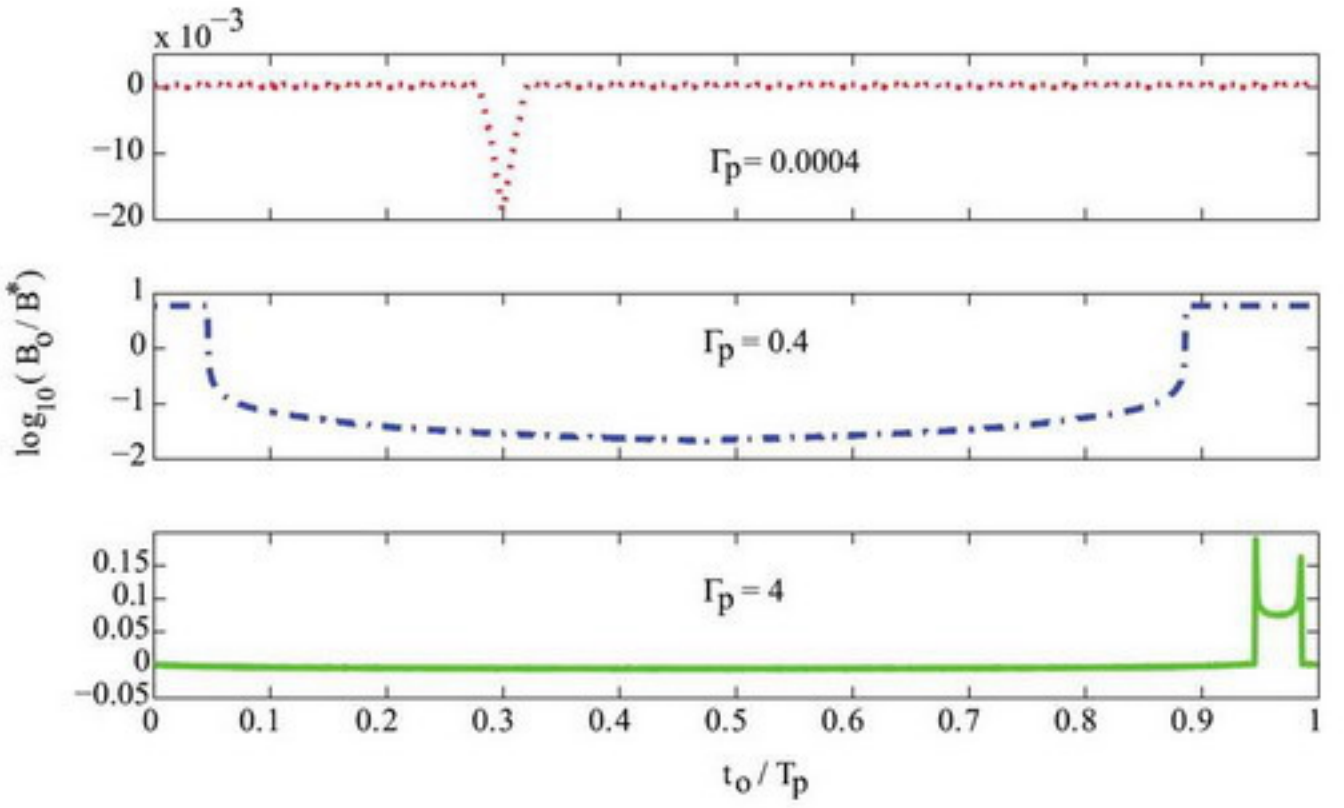

FIG. 5. (Color online) Observed light curves for different values of the parameter Γ_p in Eq. (28).

D. Photosphere vibration and apparent binaries

Different regions of the photosphere vibrations can have out-of-phase radial velocities, e.g., v_p and $-v_p$ at the same time instant (say, $t_{e,i}$). Note that such out-of-phase, radial velocities readily occur in flexural vibrational modes of thin shells—these flexural modes can have lower associated resonance frequencies than the totally symmetric breathing (fundamental) mode of vibration.[20] Consequently, photons emitted from these regions (at $t_{e,i}$) will arrive at the observer at different time instants, as in Eqs. (25) and (26),

$$t_{o,i+} = t_{e,i} + \frac{d_{e,o} - r_p(0)}{c + c\beta_p(0)}, \tag{33}$$

$$t_{o,i-} = t_{e,i} + \frac{d_{e,o} - r_p(t_e)}{c - c\beta_p(t_e)}. \tag{34}$$

This leads to a time shift $(t_{o,i-} - t_{o,i+})$ between the observed light from these two regions as illustrated in Fig. 6. The photon energy observed from each region can be different, and depend on the relative size (and energy-emission rate) of each region. Since light from both regions are observed simultaneously, the total light curve can show periodic changes that appear like binary systems. Moreover, two periodically varying, apparent velocities (red shifts) will be observed as shown in Fig. 6 since the velocities (redshifts) of each region will be different. Such effects could account for large numbers of observed spectroscopic binaries with short time periods (associated with photosphere vibrations) even though visual binaries tend to have substantially larger, time periods.

Intermediate regions between the major vibrational regions will distort the simple addition of the two shifted light curves in Fig. 6. This distortion will depend on the relative size (and energy-emission rate) of the major and intermediate regions. Moreover, the spread of redshifts could lead a time-varying thickening of the spectrum bands rather than generating discrete values in the spectrum as in the above example. Higher-order vibrational modes can lead to multiple regions with substantially different phase. This can lead to more than two, shifted, light curves being observed simultaneously resulting in apparent multiple-star systems. These issues are not considered in this study, for simplicity. Nevertheless, the proposed Ritz-type model indicates that photosphere vibration can lead to observations that appear to be from binary or multistar systems.

IV. QUASAR DISTANCE AND TIME DILATION

In this section, the cosmological expansion effect (that was neglected in Sec. III, which studied nearby stars) is included when computing the time between emission and observation. The results are used to generate potential explanations for the apparent lack of time dilation in quasar light curves,[13] as well as the observational links between quasars and nearby-galaxies.[14,15]

A. Time-dilation expression

Consider the case when a photon is emitted by a moving photosphere, which is considered to be spherical about the emitter e as in Fig. 1. Let two photons be emitted at time instants $t_{e1} = t_{e,i}$ and $t_{e2} = t_{e,i} + t_e$, which reach the observer o at time instants t_{o1} and t_{o2}, respectively. Since the center of the emitter is moving with speed $(c - c_o)$ away from the observer due to cosmological expansion, in Eq. (4), during the emission time-interval $t_e = t_{e2} - t_{e1}$, the initial distance $d(e_1, o_1)$ (between the centers of the emitter and the observer) has increased by $V_{e,o}t_e = (c - c_o)t_e$ to the final distance $d(e_2, o_2)$, as illustrated in Fig. 7. Moreover, let the radius of the photosphere, at the two emission instants, be $r_{p1} = r_p(t_{e1})$ and $r_{p2} = r_p(t_{e2})$ with expansion rates $c\beta_{p1} = c\beta_p(t_{e1})$ and $c\beta_{p2} = c\beta_p(t_{e2})$. Consequently, the photons emitted at time instants t_{e1} and t_{e2} move toward the observer at speeds $v_1 = c_o + c\beta_1$ and $v_2 = c_o + c\beta_2$,

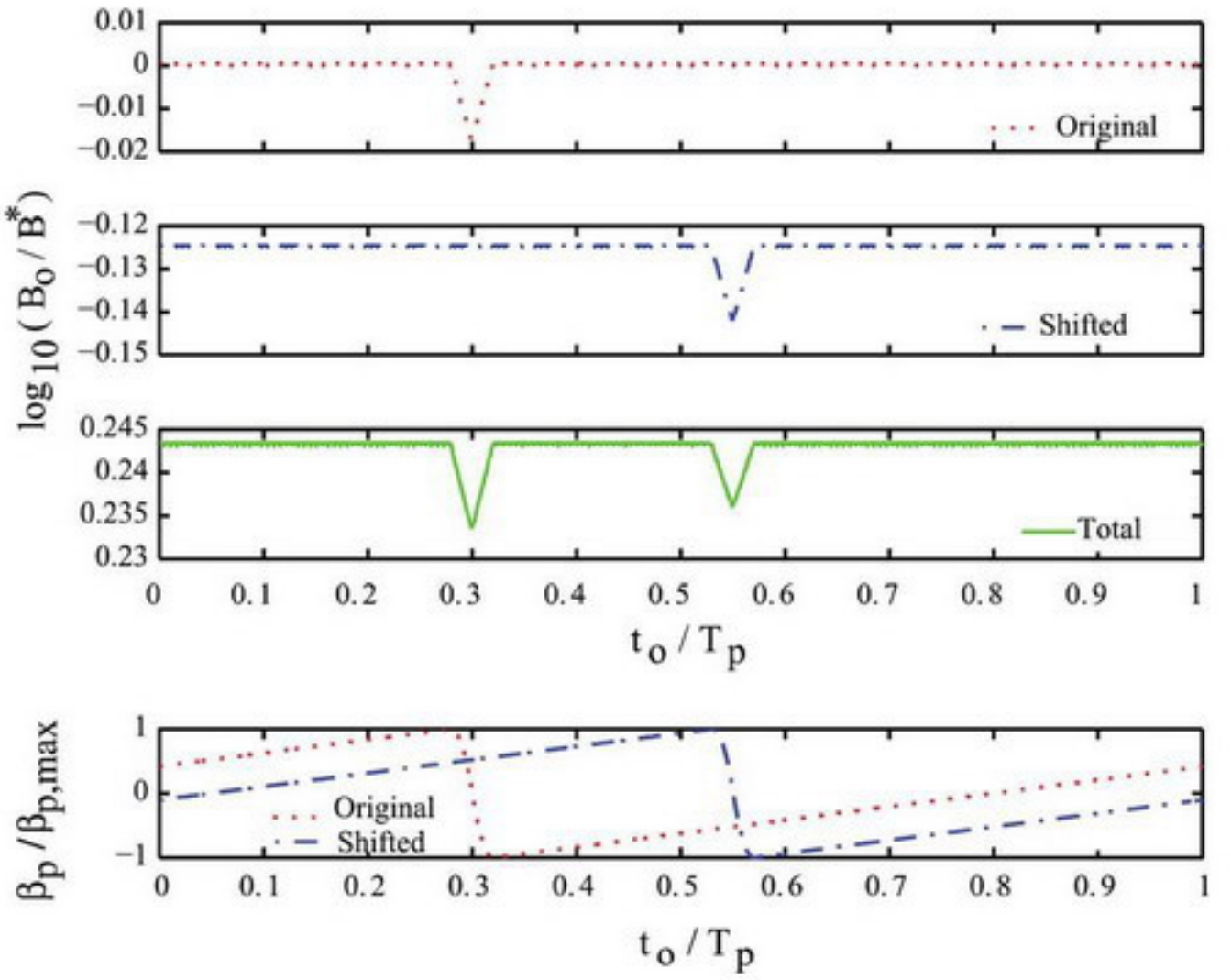

FIG. 6. (Color online) Apparent binaries: (Top three plots) Observed brightness B_o. The observed time shift (from the original brightness plot in Fig. 4) is a quarter of the time period ($T_p/4$) and the brightness of the shifted light curve is 3/4th of the original brightness. (Bottom plot) Observed photosphere speed ($\beta_p/\beta_{p,max}$), where at the same (shifted observer) time instant t_o, two values of photosphere speed can be observed, which could appear similar to observations from a spectroscopic binary.

$$t_{o1} = t_{e1} + \frac{d(e_1, o_1) - r_{p1}}{c_o + c\beta_{p1}}, \tag{35}$$

$$t_{o2} = t_{e2} + \frac{d(e_2, o_2) + (c - c_o)t_e - r_{p2}}{c_o + c\beta_{p2}}. \tag{36}$$

Therefore, the time interval t_o between observations is (provided $t_{o2} \geq t_{o1}$)

$$\begin{aligned} t_o(t_e) = t_{o2} - t_{o1} &= t_e + \frac{d(e_1, o_1) + (c - c_o)t_e - r_{p2}}{c_o + c\beta_{p2}} \\ &\quad - \frac{d(e_1, o_1) - r_{p1}}{c_o + c\beta_{p1}}, \\ &= t_e \left[1 + \frac{(1 - c_o/c)}{(c_o/c + \beta_{p2})}\right] \\ &\quad - \left[\frac{(\beta_{p2} - \beta_{p1})\frac{d(e_1, o_1)}{c}}{(c_o/c + \beta_{p2})(c_o/c + \beta_{p1})}\right] \\ &\quad - \left[\frac{(r_{p2}/c)}{(c_o/c + \beta_{p2})} - \frac{(r_{p1}/c)}{(c_o/c + \beta_{p1})}\right], \end{aligned} \tag{37}$$

which is similar to the expression in Eq. (27) for the case without cosmological expansion in Sec. III. The main difference between the two cases is in the first term, where an additional expression is present in Eq. (37) for the case with cosmological expansion. This additional term tends to zero when the cosmological redshift is small. Moreover, the observation interval t_o becomes substantially large as the distance $d(e_1, o_1)$ increases and the second term in Eq. (37) dominates the expression—even for a small change in the photosphere speed over the emission interval t_e. Large changes in the observation time interval can lead to

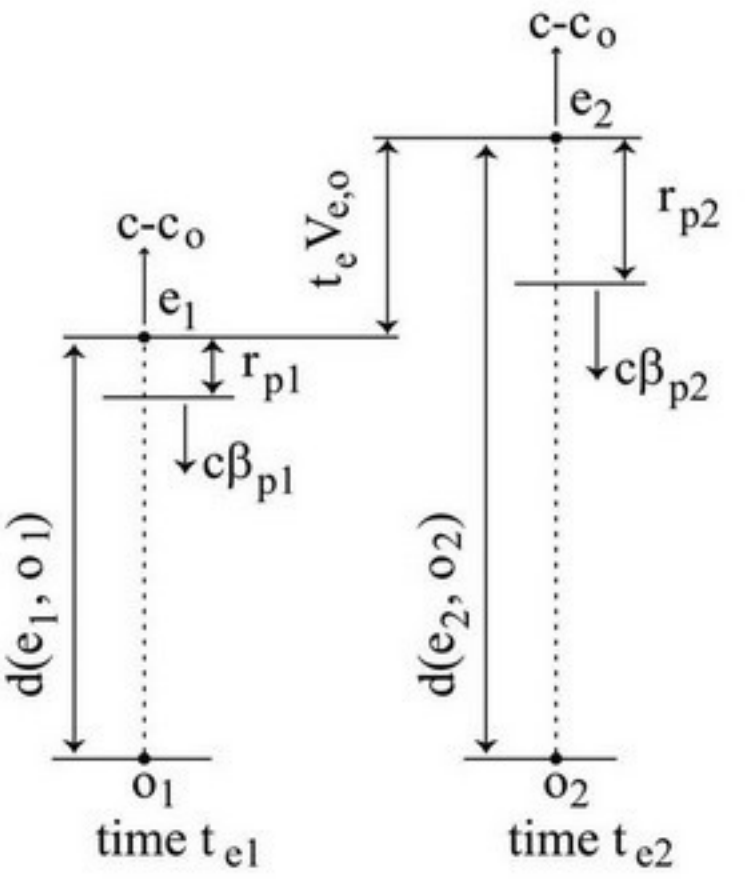

FIG. 7. Light emitted from point e_1 at time t_{e1} and from point e_2 at time $t_{e2} = t_{e1} + t_e$. The position of the photosphere is r_{p1} and r_{p2} away from the emitter center (toward the observer) and the corresponding speeds of the photosphere are $c\beta_{p1}$ and $c\beta_{p2}$. The relative speed $V_{e,o}$ of the emitter e with respect to the observer o is $(c - c_o)$. In the reference frame of the observer I_o, in which the location of the observer is fixed, i.e., $o_1 = o_2$.

redistributions of the light curve over the time period that can appear to be chaotic—similar advent of chaos has been studied in stellar dynamics, e.g., Ref. 21.

The relation between emission and observation intervals in Eq. (37) can be rewritten in terms of the cosmological redshift z using Eqs. (2), (9), (10), and (19) as

$$t_o(t_e) = t_e\left[1+\frac{z}{(1+\beta_{p2}(1+z))}\right] - \left[\frac{(\beta_{p2}-\beta_{p1})H^{-1}z}{(1+\beta_{p1}(1+z))(1+\beta_{p2}(1+z))}\right] - \left[\frac{(r_{p2}/c)(1+z)}{(1+\beta_{p2}(1+z))}-\frac{(r_{p1}/c)(1+z)}{(1+\beta_{p1}(1+z))}\right]. \quad (38)$$

Note that the second term in Eq. (38) relates to the speed variations in the photosphere and the third term includes radii variations of the photosphere. The time dilation expression in Eq. (38) collapses to the expression $t_o = (1+z)t_e$ in Eq. (12) if the photosphere radius is not varying, i.e., $r_{p1} = r_{p2}$ and the speeds β_{p1} and β_{p2} are zero.

B. Periodic pulse emissions

Consider the case, when emissions are periodic pulses occurring when the photosphere has a specific speed $c\beta_p$ and radius r_p. This could occur, for example, if the emission accompanies (periodic) collapses of the stellar system. Then, the relation in Eq. (38) between the emission and observation time intervals t_e and t_o reduces to

$$t_o = t_e\left[1+\frac{z}{1+\beta_p(1+z)}\right], \quad (39)$$

where z is the cosmological redshift. Note that this expression for time dilation in Eq. (39) is similar to that in Eq. (12)—the difference is the additional effect of the photosphere speed (i.e., β_p) at the instant the pulses are emitted in Eq. (39).

C. Spectroscopic versus cosmological redshift

The time dilation can be expressed in terms of the measured spectroscopic redshift (that includes the effect of photosphere motion, i.e., $\beta_p \neq 0$) rather than the cosmological redshift z in Eq. (9) due to cosmological expansion alone without photosphere motion, i.e., $\beta_p = 0$. Toward this, the cosmological redshift z is compared with the spectroscopic redshift z_s that is given by, similar to Eq. (9),

$$1+z_s = \frac{c}{c_o + c\beta_p}, \quad (40)$$

provided

$$c_o + c\beta_p > 0, \quad (41)$$

which is important to ensure that emitted photons have a positive speed toward (and reach) the observer. The spectroscopic redshift z_s can be related to the cosmological redshift z by using Eq. (9) as

$$1+z_s = \frac{1}{\frac{1}{1+z}+\beta_p}, \quad (42)$$

which can be rewritten as

$$(1+z) = \frac{(1+z_s)}{1-\beta_p(1+z_s)}. \quad (43)$$

The spectroscopic redshift z_s approaches infinity as the cosmological redshift z reaches a critical value z_c and the net speed of photons tends to zero. In particular, for photons to reach an observer, Eq. (41) should be satisfied, which also implies that the denominator of Eq. (42) should remain positive, i.e.,

$$(1+z)\beta_p > -1, \quad (44)$$

yielding an expression for the critical redshift z_c for a collapsing photosphere $(\beta_p < 0)$ as

$$z < z_c = \frac{1}{|\beta_p|} - 1 \quad \text{if} \quad \beta_p < 0. \quad (45)$$

D. Distance to quasars

When the photosphere speed is small, $\beta_p \to 0$, the spectroscopic redshift z_s approaches the cosmological redshift z as seen in Eq. (42). However, the spectroscopic redshift z_s can be large compared to the cosmological redshift z when $z \to z_c$ as illustrated in Fig. 8. Therefore, the Hubble law in Eq. (18) would indicate that an object is substantially further away if the spectroscopic redshift z_s is used instead of the cosmological redshift z. In other words, high spectroscopically redshifted quasars might be nearer than

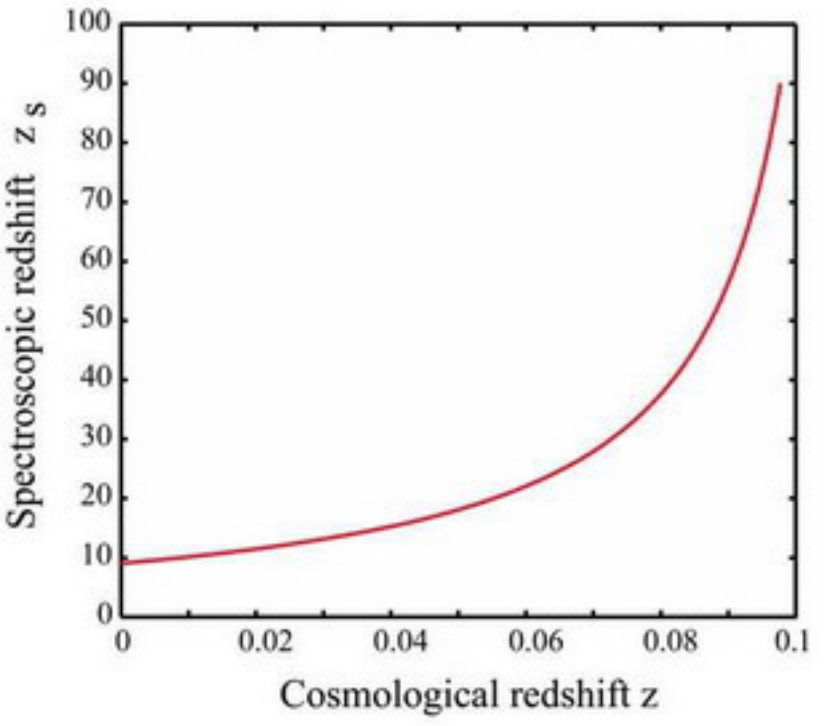

FIG. 8. (Color online) Spectroscopic z_s versus cosmological z redshift with an example photosphere speed of $v_p = -0.9c$ ($\beta_p = -0.9$). This can lead to erroneous distance (and age) estimates from the Hubble law in Eq. (18) if the spectroscopic redshift z_s is used instead of the cosmological redshift z.

previously thought, which could explain, e.g., the quasar redshift-distance anomalies such as potential links between high-(spectroscopic)-redshift quasars and lower-redshift galaxies.[14,15] If the distance is not as large as thought, then it is possible that ejecta observations at superluminal speeds[16] might be traveling at much smaller speeds—although the model presented here does not preclude superluminal speeds.

E. Quasar time dilation

The time-dilation relation in Eq. (39) between the emission and observation time intervals t_e and t_o can be expressed in terms of the spectroscopic redshift z_s as

$$\frac{t_o}{t_e} = 1 + \frac{\left[\dfrac{z_s + \beta_p(1+z_s)}{1-\beta_p(1+z_s)}\right]}{\left[1 + \dfrac{\beta_p(1+z_s)}{1-\beta_p(1+z_s)}\right]} = (1+z_s)(1+\beta_p). \quad (46)$$

Therefore, the time dilation is different by $(1+\beta_p)$ when compared to the standard expression obtained by replacing the cosmological redshift z in Eq. (12) by the spectroscopic redshift z_s, i.e.,

$$\frac{t_o}{t_e} = (1+z_s). \quad (47)$$

Thus, for a collapsing system, with large negative photosphere speeds, e.g., $\beta_p = -0.9$, the actual time dilation from Eq. (46) can be substantially lower than the time dilation predicted by the standard expression in Eq. (47) as seen in Fig. 9. This could explain recent analysis that appears to indicate that quasars do not show anticipated time dilation effects even with substantial spectroscopic redshifts.[13]

Emissions from quasar can have time dependency, which is different from the periodic pulses considered in the above analysis. Additionally, variations in the photosphere speeds can lead to more complex light curves (being observed) due to variations in the time dilation as predicted by Eq. (38)—these are not considered here for simplicity. Nevertheless, the above analysis shows the potential of the proposed model to account for the absence of time dilation in quasar light curves.[13] Moreover, the difference between the spectroscopic redshift z_s and cosmological redshift z in the proposed model could explain the anomaly between smaller apparent distance (due to potential links to low redshift galaxies as well as the presence of superluminal ejecta) and large quasar (spectroscopic) redshifts.[14–16]

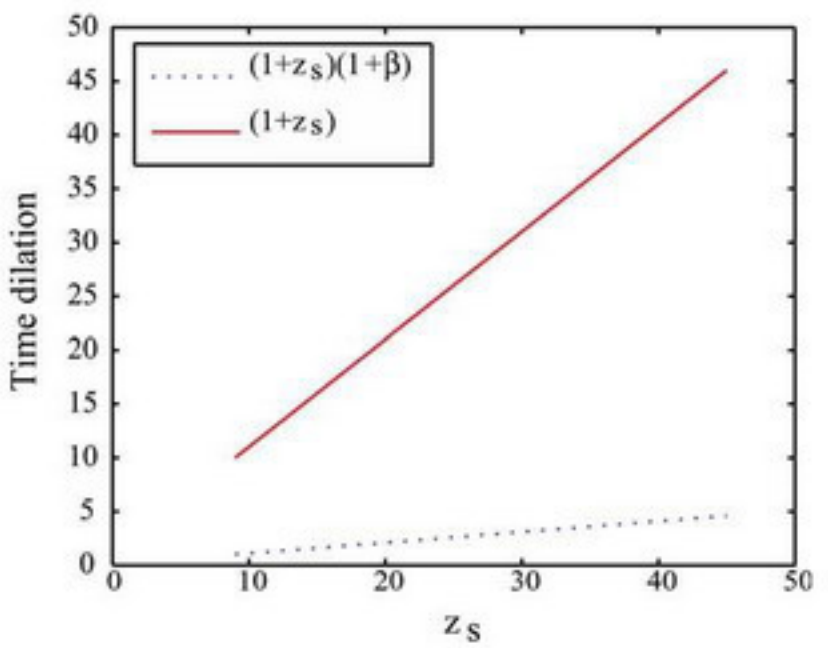

FIG. 9. (Color online) Comparison of time-dilation predictions. Time dilation predictions (solid line) based on the spectroscopic redshift z_s as in Eq. (47) can be substantially higher than the time-dilation (dotted line) based on the proposed model in Eq. (46). The difference depends on the photosphere speed, which is $v_p = -0.9c$ ($\beta_p = -0.9$) for this plot.

V. CONSISTENCY WITH FARTHER-DIMMER EFFECT

The effect of photosphere-speed variation is evaluated as a potential explanation of the farther–dimmer effect in SNe observations.[17]

A. Effect of speed variation on time dilation

Consider the case when the photosphere speed $c\beta_p$ varies slightly over the time interval t_e. Then, the observed time dilation expression in Eq. (38) can be simplified by setting $\beta_{p1} = \beta_p$, $\beta_{p2} = \beta_p + \alpha_p t_e$, and $\beta_{p2} - \beta_{p1} = \alpha_p t_e$, where α_p is the normalized photosphere acceleration. The overall photosphere changes are assumed to be small, i.e.,

$$1 + \beta_{p2}(1+z) \approx 1 + \beta_{p1}(1+z) \approx 1 + \beta_p(1+z), \quad (48)$$

and $r_{p2} \approx r_{p1} + c\beta_p t_e$, to obtain

$$t_o(t_e) \approx t_e(1+z)\frac{\left[1 - \left(\dfrac{z}{1+z}\right)\dfrac{\alpha_p H^{-1}}{1+\beta_p(1+z)}\right]}{\left[1+\beta_p(1+z)\right]}. \quad (49)$$

B. Modified Hubble law

Substituting the modified time-dilation expression in Eq. (49) into the derivation of the observed brightness, i.e., in Eq. (15), the observed brightness of SNe B_{SN}, i.e., B_o in Eq. (16), can be rewritten as

$$B_{SN} = \frac{L_e}{4\pi\left(\dfrac{Rc}{V}\right)^2\left(\dfrac{z^2}{1+z}\right)} \times \left[\frac{1+\beta_p(1+z)}{(1+z)\left[1 - \left(\dfrac{z}{1+z}\right)\dfrac{\alpha_p H^{-1}}{1+\beta_p(1+z)}\right]}\right] = \frac{L_e}{4\pi(d_{L,SN})^2}, \quad (50)$$

with the following modified Hubble law in Eq. (18) for SNe observations due to changes in the photosphere speed (represented by the term α_p):

$$d_{L,SN} = \frac{Rc}{V} z \sqrt{\frac{1 - \left(\dfrac{z}{1+z}\right)\dfrac{\alpha_p H^{-1}}{1+\beta_p(1+z)}}{1+\beta_p(1+z)}}, \quad (51)$$

where $d_{L,SN}$ is the luminosity distance for supernova observations. For small photosphere speeds (e.g., $\beta_p = 0.033$ (Ref. 22)), the above expression can be simplified, further, to

$$d_{L,SN} \approx \frac{Rc}{V} z \sqrt{1 - \left(\frac{z}{1+z}\right)\alpha_p H^{-1}}. \tag{52}$$

C. Farther dimmer with decelerating photosphere

If the photosphere acceleration is negative $(\alpha_p < 0)$, then the time dilation in Eq. (49) is increased—this results in an increase in the luminosity distance, e.g., in Eq. (52). This offers a potential explanation of the farther–dimmer effect,[17] as discussed below.

Based on the Hubble law in Eq. (18), the variation of the observed (normalized) blue-band maximum μ_B from supernova (Type 1a) observations as a function of the host-galaxy redshift can be expressed in terms of the luminosity distance d_L (or, rather, the redshift z) as

$$\mu_B = K_B + 5\log_{10}\left[\frac{V}{Rc} d_L\right] = K_B + 5\log_{10}[z], \tag{53}$$

where K_B is a constant. This does not match the observed data from the Supernova Cosmology Project (SCP)[23] as shown in Fig. 10—leading to the possibility of an accelerating universe.

With the proposed model, the variation of observed maximum light can be expressed in terms of the luminosity distance $d_{L,SN}$ from Eq. (51)

$$\begin{aligned}\mu_B &= K_B + 5\log_{10}\left[\frac{V}{Rc} d_{L,SN}\right] \\ &= K_B + 5\log_{10}\left[z\left[\frac{1 - \left(\frac{z}{1+z}\right)\frac{\alpha_p H^{-1}}{1+\beta_p(1+z)}}{1+\beta_p(1+z)}\right]^{1/2}\right],\end{aligned} \tag{54}$$

which reduces to, at small photosphere speeds, $\beta_p \to 0$,

$$\mu_B(z) = K_B + 5\log_{10}\left[z\left(1 - \frac{z}{1+z}\alpha_p H^{-1}\right)^{1/2}\right]. \tag{55}$$

The parameters $K_B = 43.13$ and $\alpha_p H^{-1} = -3.18$ were estimated by minimizing the least square error between the model's prediction from Eq. (54) and the observed data ($N_{SCP} = 307$ pairs of blue-band maximum $\mu_{B,i}$ and redshift z_i with index $i = 1, ..., N_{SCP}$) from the SCP[23] at an example photosphere speed of $\beta_p = 0.033$.[22] The residual error $E_{SCP,i}$ between the observed blue-band maximum $\mu_{B,i}$ and the predictions $\mu_B(z_i)$ from Eq. (55) at the observed redshift z_i is defined as

$$E_{SCP,i} = \mu_{B,i} - \mu_B(z_i). \tag{56}$$

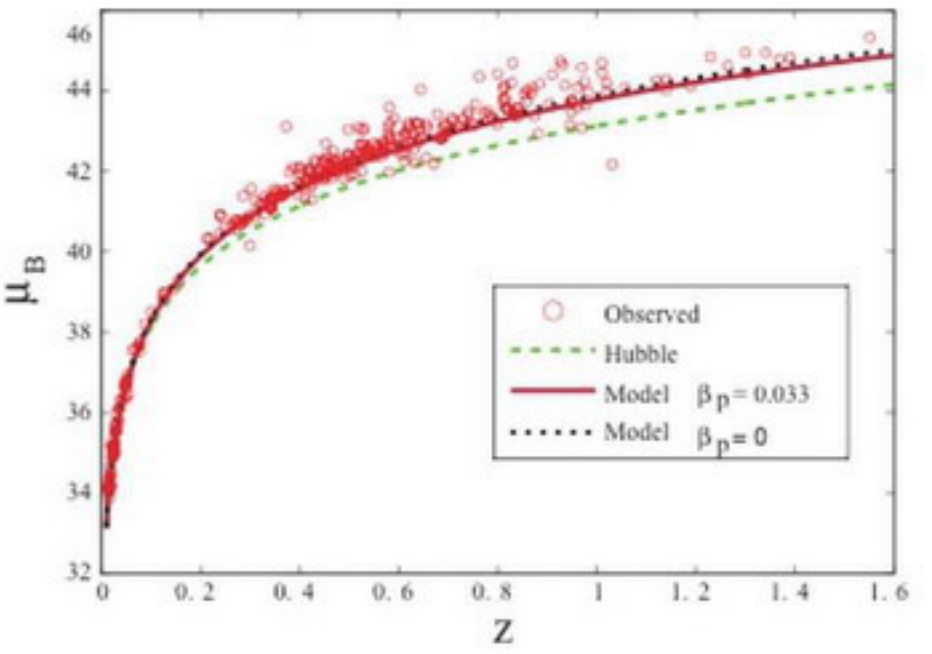

FIG. 10. (Color online) Hubble diagram (solid line) with the photosphere motion model in Eq. (51) with $\beta_p = 0.033$ captures the farther–dimmer relationship in supernova observations (circles) when compared to the predictions in Eq. (53) (dashed line) from the standard Hubble law. The prediction from the simplified model in Eq. (55) with $\beta_p = 0$ is shown for comparison—the simplified prediction varies by less than 0.1 from the model with the nominal photosphere speed of $\beta_p = 0.033$. The circles represent 307 SNe data (that are not outliers) from the SCP [23].

The error norm E_{SCP},

$$E_{SCP} = \sqrt{\sum_{i-1}^{N_{SCP}} \left[E_{SCP,i}\right]^2}, \tag{57}$$

over all observations is plotted for different values of K_B and $\alpha_p H^{-1}$ in Fig. 11. The central ellipse in Fig. 11 represents the minimum of the error norm E_{SCP}, which led to parameter estimates of $K_B = 43.13$ and $\alpha_p H^{-1} = -3.18$. The resulting residual error $E_{SCP,i}$ as in Eq. (56), shown in Fig. 11, has low correlation with the redshift—the correlation $R_{residual}$ between the residual error $E_{SCP,i}$ and the redshift z_i is $R_{residual} = -0.0173$ with a 95% confidence interval $(-0.1290, 0.0948)$. Thus, the proposed model can account for the farther–dimmer relationship in supernova observations,[17] without an accelerating universe.

VI. TEMPORAL AND SPATIAL DISTORTIONS

Variations in the speed of photons can cause temporal and spatial distortions in astronomical observations. Such distortions are discussed below for two cases: (i) temporal distortion in SNe light curves and (ii) spatial distortion of mass distribution in galaxies.

A. Temporal distortion in SNe light curves

An aspect of the proposed model is the potential for apparent time reversal. In Sec. V C, deceleration of the photosphere was shown to result in different photon speeds, which in turn, causes additional time dilation. A similar effect is possible, even with an accelerating photosphere due to apparent time reversal. In particular, a photon emitted at time t_{e2} could be observed earlier than a photon emitted earlier at time $t_{e1} < t_{e2}$. Let the corresponding observation times be t_{o1} (photon emitted earlier) and t_{o2} with $t_{o1} > t_{o2}$ as in

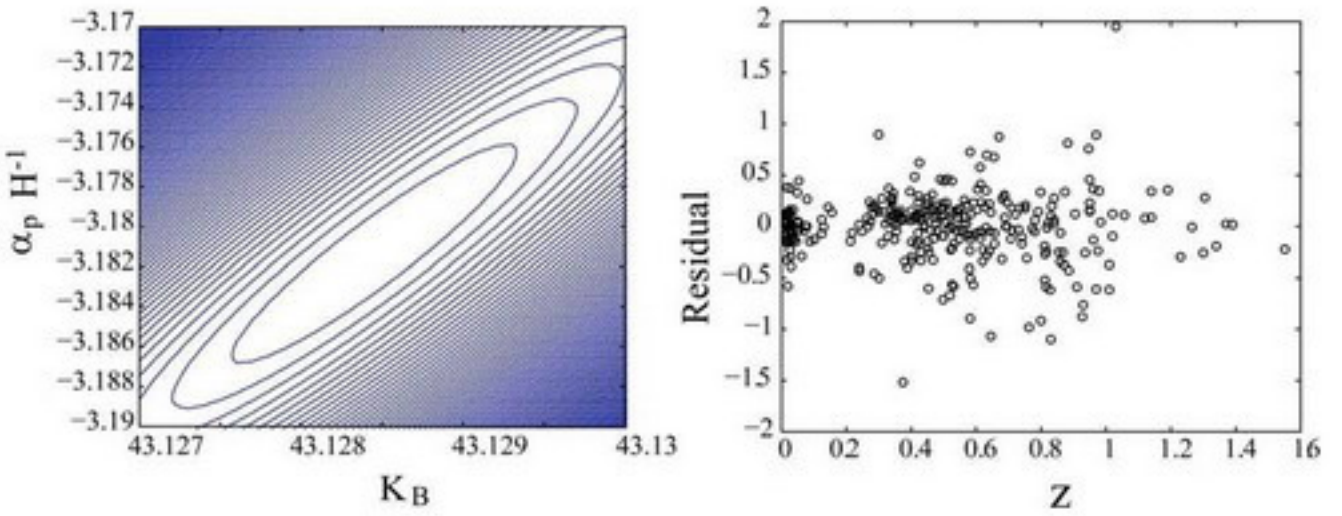

FIG. 11. (Color online) Left error norm E_{SCP} from Eq. (57) for different model parameters K_B and $\alpha_p H^{-1}$ from Eq. (55). The central ellipse in Fig. 11 represents the minimum of the error norm E_{SCP}, which led to parameter estimates of $K_B = 43.13$ and $\alpha_p H^{-1} = -3.18$. Right: the resulting residual error $E_{SCP,i}$ in Eq. (56) has low correlation, $R_{residual} = -0.0173$, with redshift z_i.

Eq. (36). In this case, the time interval t_o between observations is, reversing the observation time intervals t_{o1} and t_{o2} in Eq. (37),

$$\begin{aligned} t_o(t_e) &= t_{o1} - t_{o2} \\ &= -t_e - \frac{d(e_1,o_1) + (c - c_o)t_e - r_{p2}}{c_o + c\beta_{p2}} \\ &\quad + \frac{d(e_1,o_1) - r_{p1}}{c_o + c\beta_{p1}}, \\ &= -t_e \left[1 + \frac{(1 - c_o/c)}{(c_o/c + \beta_{p2})}\right] \\ &\quad + \left[\frac{(\beta_{p2} - \beta_{p1})\dfrac{d(e_1,o_1)}{c}}{(c_o/c + \beta_{p2})(c_o/c + \beta_{p1})}\right] \\ &\quad + \left[\frac{(r_{p2/c})}{(c_o/c + \beta_{p2})} - \frac{(r_{p1/c})}{(c_o/c + \beta_{p1})}\right], \end{aligned} \tag{58}$$

which can be positive $t_o(t_e) > 0$ with an accelerating photosphere provided the second term in Eq. (58) is positive and dominates the other two terms in Eq. (58), i.e., the speed of the later photon β_{p2} is greater than the speed β_{p1} of the earlier photon, there is sufficient travel distance $d(e_1,o_1)$ for the later photon to overtake the earlier photon, and there is no interference between the photons.

The apparent time reversal can lead to SNe light with the highest photosphere speeds to be observed first, with a continuous decrease in the observed photosphere speed over time—such a reduction in photosphere speed is present in current SNe observations.[22] Moreover, if the photosphere was accelerating during the explosion, the apparent time reversal can lead to apparent reversal in the direction of the observed shock waves, i.e., they might appear to propagate backward toward the supernova center. Further study is needed to evaluate if the reverse shock waves, seen in some of the SNe remnants,[24] could be caused by such an effect. Finally, apparent time reversal also implies that light from the host galaxy (which might not have the large photosphere velocities as SNe) travel at a slower speed when compared to the associated SNe. Consequently, the light from the host galaxy (observed at the same time as the SNe) can be much older than the SNe. This difference in age (between SNe and their host galaxies) could account for the difficulty in identifying SNe progenitors.[25]

B. Spatial distortion of astronomical structures

Variations in the arrival speed (of photons) can lead to distortions in the observed mass distribution of astronomical structures such as galaxies. If not accounted for, apparent spatial distortions can raise challenges in modeling the dynamics of observed physical phenomena such as the rotational dynamics of galaxies, which are dependent on the mass distribution. To illustrate, consider an astronomical structure, illustrated by the disk in Fig. 12 that is rotating about an axis EO that passes through the disk center E and is perpendicular to the disk. Consider light emitted from a point A on the disk, which is at a distance $r = d(E,A)$ from the disk center E with tangential speed $V_g(r) = c\beta_g(r)$. Let the observer be at location O, where the distance $d = d(E,O)$ is large compared to the radius r, which allows the approximation $d(A,O) \approx d$. Then, the time $t(r)$ for a photon to travel to the observer at O is given by

$$\begin{aligned} t(r) &= \frac{d(A,O)}{c_g} \\ &= \frac{d(A,O)}{c\sqrt{1 - \left[\beta_g(r)\right]^2}} \approx \frac{d}{c\sqrt{1 - \left[\beta_g(r)\right]^2}}, \end{aligned} \tag{59}$$

where cosmological expansion effects are neglected in the relative speed of light c_g. The difference between the travel times for emission from the center E and the emission from the point A is given by

$$\begin{aligned} \Delta t(r) &= t(r) - t(0) \\ &= \frac{d}{c\sqrt{1 - \left[\beta_g(r)\right]^2}} - \frac{d}{c} \\ &= \frac{d}{c}\left[\frac{1 - \sqrt{1 - \left[\beta_g(r)\right]^2}}{\sqrt{1 - \left[\beta_g(r)\right]^2}}\right]. \end{aligned} \tag{60}$$

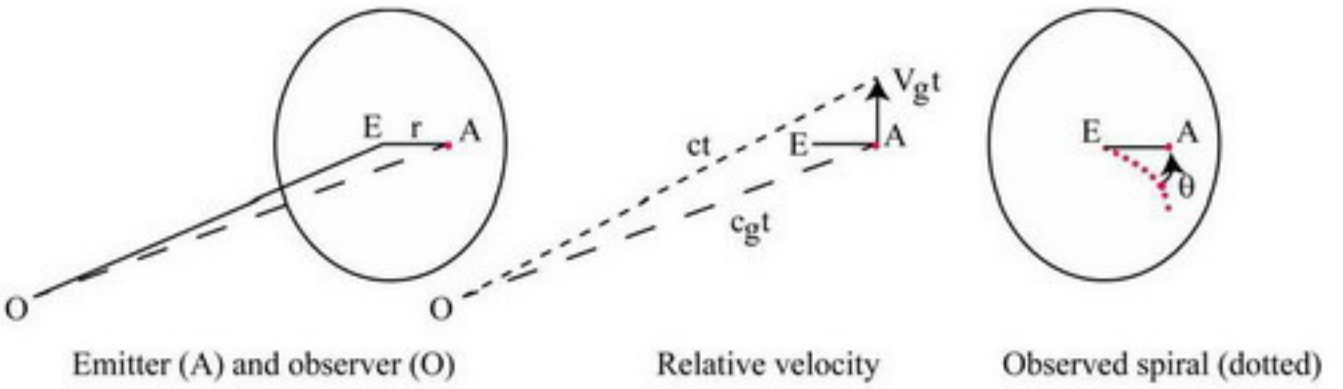

FIG. 12. (Color online) Spiral spatial distortion. Travel times for emissions from A on a disk at radial distance r from the disk center E can vary with the radial distance d as in Eq. (59)—this can lead to the straight segment EA appearing as a spiral when observed at O.

The above expression can be simplified, for small tangential speeds $(\beta_g(r) \to 0)$, as

$$\Delta t(r) = \frac{d}{c}\left[\frac{\left[\beta_g(r)\right]^2}{2}\right]. \tag{61}$$

Note that the travel-time difference can be a function of the radial distance r from the center E, which can imply different angular rotations $\theta(r)$ before an emission reaches the observer. In particular, if the angular rotation rate $\omega(r)$ at each radius r is assumed to remain constant, then the time difference in Eq. (61) corresponds to a rotation angle $\theta(r)$ given by

$$\theta(r) = \omega(r)\Delta t(r) = \frac{c\beta_g(r)}{r}\left[\frac{d}{c}\frac{\left[\beta_g(r)\right]^2}{2}\right] = \frac{d}{2r}\left[\beta_g(r)\right]^3. \tag{62}$$

If, for example, the disk rotates as a rigid body at a constant angular rate ω, then the tangential speed is given by

$$c\beta_g(r) = r\omega, \tag{63}$$

and the corresponding angular rotation $\theta(r)$ during the travel time difference $\Delta t(r)$ is given by

$$\theta(r) = \frac{d}{2r}\left[\frac{r\omega}{c}\right]^3 \propto r^2. \tag{64}$$

Therefore, a straight line along the radius of the disk (e.g., EA) will appear to be a spiral due to increasing travel times for emissions along the length EA—as illustrated in Fig. 12. Such spatial distortion in observations needs to be corrected before studying the rotational dynamics since it can affect the mass distribution in the disk, and therefore, can affect the gravitational analysis. Similar spatial distortion can also occur along other directions such as the radial direction, e.g., in the presence of varying radial speeds if the disk collapses or expands, which will require further investigation.

VII. THE GEOMETRY AXIOM

The spherical-shell geometry axiom allows for the total kinetic energy to be constant while satisfying momentum conservation. The implications and potential relaxation of this axiom are discussed below.

A. Peculiar velocities

The expansion rate is simplified to be a constant V (which maintains a constant kinetic energy) in the proposed cosmology model in contrast to a radial-distance-dependent speed variation as in Newtonian cosmology, e.g., Ref. 18. Nevertheless, a small expansion-rate variation across the thickness of the shell could be included in the proposed cosmology model. For example, components on the outside of the shell will have a net gravitational force toward the center of the shell—in contrast, there would be no such force on components on the inside of the shell. Therefore the speed V of the outer components in the shell (farther away from the center) is expected to reduce with respect to the inner components in the shell that are nearer to its center. Therefore, the inner components of the shell might appear to be attracted toward the outside components, which could explain observations such as peculiar velocities of galaxy clusters.[26]

B. Anisotropy in cosmic microwave background radiation

The spherical shell geometry leads to variation between the radial and tangential directions. Moreover, even within the radial direction, there is anisotropy between the directions toward the center and away from the center. This should lead to anisotropy in observations such as the measured Hubble constant in different directions and in observations of the cosmic microwave background (CMB) radiation. Although some anisotropies have been reported in measurements of: (i) the Hubble constant (e.g., Ref. 27) and (ii) CMB radiation (e.g., quadrupole and octopole alignment[28,29]) further study is needed to check if such anisotropies are consistent with the proposed cosmology model.

C. Other geometries

If anisotropies in cosmological observations are not observed, then the proposed cosmology model can be considered without the spherical-shell geometry axiom. In this case, the Hubble law cannot be derived as in Sec. II under the proposed model. Therefore, the expansion of the cosmos should be considered as an axiom, as in current cosmology models. Nevertheless, the other results of the model, such

as the explanation of apparent binaries in Sec. III, the farther–dimmer effect in Sec. V, and the temporal-and-spatial distortions in Sec. VI, would still be viable.

VIII. CONCLUSIONS

This article developed a Ritz-type, VSL cosmology model, and evaluated its potential to match current cosmological observations. It was shown that the proposed model could explain some of the anomalies in current cosmological observations. Additional work is needed to evaluate potential variations in the Hubble constant and anisotropies in the CMB radiation due to differences between the radial and tangential directions in the spherical shell geometry to, both, test and potentially refine the model.

[1]M. H. Shao, Phys. Essays **26**, 183 (2013).
[2]D. Laskaroudis, Phys. Essays **26**, 452 (2013).
[3]W. Petry, Phys. Essays **26**, 315 (2013).
[4]L. Zaninetti, Phys. Essays **23**, 298 (2010).
[5]R. B. Driscoll, Phys. Essays **23**, 584 (2010).
[6]A. A. Martinez, Phys. Perspect. **6**, 4 (2004).
[7]J. P. Petit, Mod. Phys. Lett. A **3**, 1733 (1988).
[8]S. Devasia, Z. Naturforsch. **64a**, 327 (2009).
[9]A. K. T. Assis and H. T. Silva, Pramana J. Phys. **55**, 393 (2000).
[10]J. J. Turin and H. R. Crane, Phys. Rev. **52**, 610 (1937).
[11]C. D. Ellis and W. A. Wooster, Proc. R. Soc. London, Ser. A, **117**, 109 (1927).
[12]S. Blondin, T. M. Davis, K. Krisciunas, B. P. Schmidt, J. Sollerman, W. M. Wood Vasey, A. C. Becker, P. Challis, A. Clocchiatti, G. Damke, A. V. Filippenko, R. J. Foley, P. M. Garnavich, S. W. Jha, R. P. Kirshner, B. Leibundgut, W. Li, T. Matheson, G. Miknaitis, G. Narayan, G. Pignata, A. Rest, A. G. Riess, J. M. Silverman, R. C. Smith, J. Spyromilio, M. Stritzinger, C. W. Stubbs, N. B. Suntzeff, B. E. Tonry, J. L. Tucker, and A. Zenteno, Astrophys. J. **682**, 724 (2008).
[13]M. R. S. Hawkins, Mon. Not. R. Astron. Soc. **405**, 1940 (2010).
[14]H. C. Arp, *Quasars, Redshifts and Controversies* (Cambridge University Press, Cambridge, UK, 1987).
[15]M. Lopez-Corredoira and C. M. Gutierrez, Astron. Astrophys. **461**, 393 (2007).
[16]M. H. Cohen, K. I. Kellermann, D. B. Shaffer, R. P. Linfield, A. T. Moffet, J. D. Romney, G. A. Seielstad, I. I. K. Paulinytoth, E. Preuss, A. Witzel, R. T. Schilizzi, and B. J. Geldzahler, Nature **268**, 405 (1977).
[18]A. G. Riess, A. V. Filippenko, W. Li, and B. P. Schmidt, Astron. J. **118**, 2668 (1999).
[19]A. R. Thatcher, Eur. J. Phys. **3**, 202 (1982).
[20]E. Hubble, Astrophys. J. **84**, 517 (1936).
[21]T. A. Duffey, J. E. Pepin, A. N. Robertson, M. L. Steinzig, and K. Coleman, J. Vib. Acoust. **129**, 363 (2007).
[22]V. Icke, A. Frank, and A. Heske, Astron. Astrophys. **258**, 341 (1992).
[23]E. C. Pearce, S. A. Colgate, and A. G. Petschek, Astrophys. J. **325**, L33 (1988).
[24]M. Kowalski, D. Rubin, G. Aldering, R. J. Agostinho, A. Amadon, R. Amanullah, C. Balland, K. Barbary, G. Blanc, P. J. Challis, A. Conley, N. V. Connolly, R. Covarrubias, K. S. Dawson, S. E. Deustua, R. Ellis, S. Fabbro, V. Fadeyev, X. Fan, B. Farris, G. Folatelli, B. L. Frye, G. Garavini, E. L. Gates, L. Germany, G. Goldhaber, B. Goldman, A. Goobar, D. E. Groom, J. Haissinski, D. Hardin, I. Hook, S. Kent, A. G. Kim, R. A. Knop, C. Lidman, E. V. Linder, J. Mendez, J. Meyers, G. J. Miller, M. Moniez, A. M. Mouro, H. Newberg, S. Nobili, P. E. Nugent, R. Pain, O. Perdereau, S. Perlmutter, M. M. Phillips, V. Prasad, R. Quimby, N. Regnault, J. Rich, E. P. Rubenstein, P. Ruiz-Lapuente, F. D. Santos, B. E. Schaefer, R. A. Schommer, R. C. Smith, A. M. Soderberg, A. L. Spadafora, L. G. Strolger, M. Strovink, N. B. Suntzeff, N. Suzuki, R. C. Thomas, N. A. Walton, L. Wang, W. M. Wood-Vasey, and J. L. Yun, Astrophys. J. **686**, 749 (2008).
[25]K. Heng, R. McCray, S. A. Zhekov, P. M. Challis, R. A. Chevalier, A. P. S. Crotts, C. Fransson, P. Garnavich, R. P. Kirshner, S. S. Lawrence, P. Lundqvist, N. Panagia, C. S. J. Pun, N. Smith, J. Sollerman, and L. Wang, Astrophys. J. **644**, 959 (2006).
[26]M. Livio and J. E. Pringle, Astrophys. J. Lett. **740**, 1 (2011).
[27]A. Kashlinsky, F. Atrio-Barandela, D. Kocevski, and H. Ebeling, Astrophys. J. **686**, L49 (2008).
[28]M. L. McClure and C. C. Dyer, New Astron. **12**, 533 (2007).
[29]M. Tegmark, A. de Oliveira-Costa, and A. J. S. Hamilton, Phys. Rev. D **68**,(2003).
[31]C. L. Bennett, R. S. Hill, G. Hinshaw, D. Larson, K. M. Smith, J. Dunkley, B. Gold, M. Halpern, N. Jarosik, A. Kogut, E. Komatsu, M. Limon, S. S. Meyer, M. R. Nolta, N. Odegard, L. Page, D. N. Spergel, G. S. Tucker, J. L. Weiland, E. Wollack, and E. L. Wright, Astrophys. J. Suppl. Ser. **192**, 1 (2011).